Multiaxial 3D MRI of the Ankle

Advanced High-Resolution Visualization of Ligaments, Tendons, and Articular Cartilage

Benjamin Fritz, MD, PD[a,b], Cesar de Cesar Netto, MD, PhD[c], Jan Fritz, MD, PD, RMSK[d,*]

KEYWORDS

• MRI • 3D • 2D • Postprocessing • Multiplanar reformation
• Curved planar reformation • Ligaments • Tendons

KEY POINTS

- 3D MRI is a newer, clinically available MRI technique for high-resolution ankle MRI with isotropic voxel size and up to five times thinner image slices.
- Clinical 3D MRI of the ankle resolves the smallest anatomic ankle structures and abnormalities of ligaments, tendons, osteochondral lesions, and nerves.
- 3D MRI postprocessing permits limitless oblique planar reformations for visualizing oblique ligaments in profile and curved planner reformations for unfolding multidirectional tendons into one image plane.

INTRODUCTION

MRI is accurate for diagnosing acute and chronic ankle conditions due to its high soft tissue contrast and resolving soft structures in high spatial resolution.[1] Clinical MRI protocols typically consist of 5–6 pulse sequences in different plane orientations and with different image contrast, including proton density, T2, and T1 weightings. In addition, those pulse sequences may be acquired without or with fat suppression.

Proton density-weighted MR images provide high morphological detail and contrast resolution for detecting and characterizing structural abnormalities of cartilage, ligaments, and tendons. Fat-suppressed fluid-sensitive proton density and T2-weighted

[a] Department of Radiology, Balgrist University Hospital, Forchstrasse 340, Zurich 8008, Switzerland; [b] Faculty of Medicine, University of Zurich, Zurich, Switzerland; [c] Department of Orthopaedics and Rehabilitation, University of Iowa, 200 Hawkins Drive, Iowa City, IA 52242, USA; [d] Department of Radiology, Division of Musculoskeletal Radiology, NYU Grossman School of Medicine, 660 1st Avenue, New York, NY 10016, USA
* Corresponding author.
E-mail address: jan.fritz@nyulangone.org

Foot Ankle Clin N Am 28 (2023) 529–550
https://doi.org/10.1016/j.fcl.2023.05.008 **foot.theclinics.com**

MR images emphasize bone marrow and soft tissue edema, joint effusions, fluid collections, hematomas, and masses. T1-weighted MR images are fat-specific and thus predominantly used for evaluating bone marrow evaluation in cases with suspected osteomyelitis and neoplastic disease. T1-weighted MR images show non-displaced fractures; however, the combination of proton density-weighted MR images and fat-suppressed fluid-sensitive MR images demonstrate non-displaced fractures with similar accuracy.[2] T1-weighted MR images without and with fat suppression are the standard to visualize intravenous gadolinium contrast enhancement.

The most commonly employed clinical MRI technique for imaging the ankle is two-dimensional (2D) MRI (**Fig. 1**), utilizing various, separately acquired fast spin-echo or turbo spin-echo pulse sequences in standardized axial, coronal, and sagittal plane orientations. These standard orthogonal plane sequences can be supplemented with individually angulated sequences to structures of particular interest, such as the anterior inferior talofibular ligament, the calcaneofibular ligament, and the flexor and peroneal tendons to achieve single plane profile views and improve their visibility. As each pulse sequence of a 2D MRI protocol has to be acquired separately, the entire 2D MRI protocol for the ankle can be time-consuming, with total acquisition times of up to 25 minutes commonly found in clinical practice.[3–5] While new acceleration techniques and artificial intelligence-driven image reconstruction can dramatically reduce the scan times of 2D MRI,[6–11] there are limitations of 2D MRI in the ankle.

2D fast spin-echo and turbo spin-echo MRI sequences provide high signal-to-noise ratios and high in-plane and contrast resolutions. However, in clinical practice, the slice thickness of 2D MRI is inherently limited to 2–3 mm, which produces partial volume averaging of small anatomic structures resulting in blurred contours of oblique

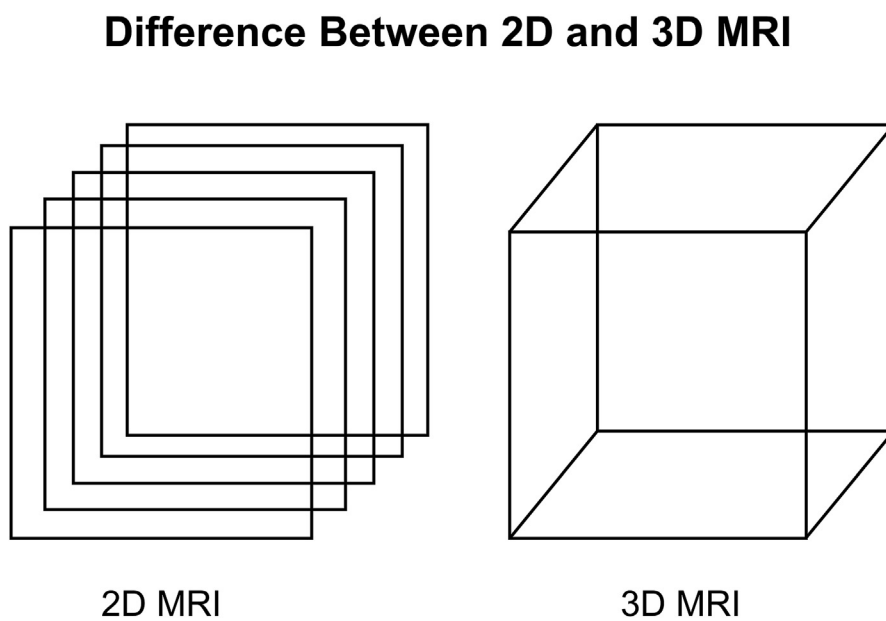

Fig. 1. Difference between two-dimensional and three-dimensional MRI. Two-dimensional MRI is acquired slice by slice, whereas 3D MRI is acquired as a single volume of small isotropic voxels. Two-dimensional MRI slices are fixated in space and may not be altered after the acquisition. As three-dimensional MRI consists of a single volume of small voxels, curved and planar slices can be created in infinite spatial orientations during postprocessing.

structures due to volume averaging effects within the image slice. This phenomenon is known as the "partial volume effect" and occurs when the size of voxel elements spans different tissues and structures, such as small ligament fibers and surrounding fat tissue or cartilage and adjacent bone (**Figs. 2** and **3**). As a result, the signals from each tissue or structure within that voxel will be mathematically combined, leading to the inability to resolve or display small anatomic structures. In some instances, this effect can also lead to the omission of subtle abnormalities in MR images.

Three-dimensional (3D) MRI is a newer, clinically available MRI technique capable of high-resolution ankle MRI, overcoming several limitations of 2D MRI.[12] While 2D MRI acquisitions are slice-by-slice, 3D MRI acquires the ankle as an entire high-resolution volume consisting of multiple voxels with symmetric edge lengths in all three spatial directions (isotropic voxels) (see **Fig. 1**). Modern clinical 3D MRI sequences allow isotropic voxels to resolve small anatomic structures and abnormalities, limit partial volume effects, and provide near-limitless multiplanar and multiaxial image reformation and postprocessing capabilities.

3D fast and turbo spin-echo MRI pulse sequences are preferable to gradient echo-based 3D MRI pulse sequences due to their better contrast resolution for bone and musculoskeletal soft tissues.[4] The primary use of gradient echo-based 3D pulse

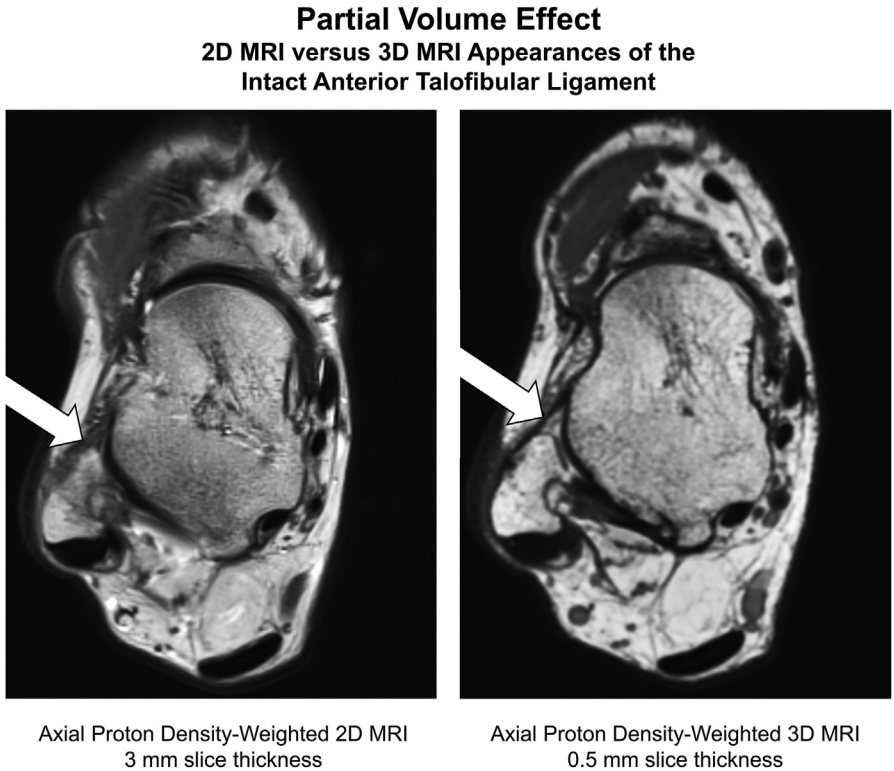

Fig. 2. Partial volume effect on 2D versus 3D ankle MRI. The 2D MR image (*left image*) is inherently prone to partial volume effect due to the thicker slices, which obscures fine detail of the intact anterior talofibular ligament (*arrow left image*). The 3D MR image (*right image*) minimizes such partial volume effects due to six times thinner slices, resulting in a sharply delineated ligament (*arrow right image*).

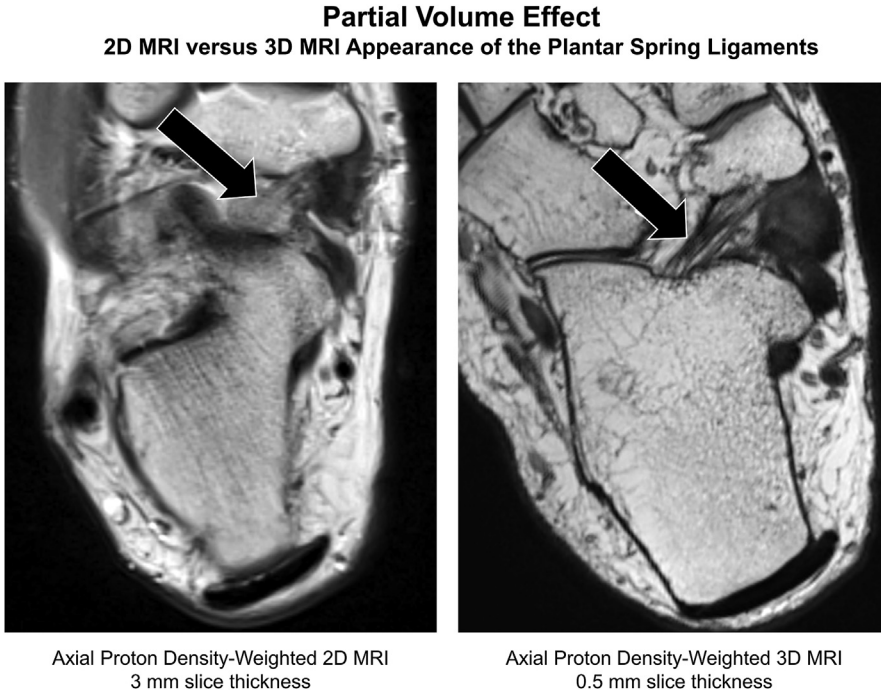

Fig. 3. Partial volume effect on 2D versus 3D ankle MRI. The 2D MR image (*left image*) is inherently prone to partial volume effect due to the thicker slices and stricty axial plane orientation, which obscures fine detail of the intact plantar spring ligaments (*arrow left image*). The 3D MR image (*right image*) minimizes such partial volume effects due to six times thinner slices and individually aligned slice along the axis of the ligament, resulting in perfect profile view with sharply delineated ligament fibers (*arrow right image*).

sequences is cartilage imaging since the lack of true T2-contrast often hampers the assessment of tendons, ligaments, and bone structures. Therefore, fast and turbo spin echo pulse sequences became the standard in musculoskeletal 3D MRI because they are not just limited to cartilage assessment but effectively evaluate all musculoskeletal tissues, including ligaments, tendons, bone marrow, and nerves.[13]

3D fast and turbo spin-echo MRI pulse sequences capable of producing true isotropic 3D data sets with similar contrast to 2D MRI were developed over 20 years ago.[14] Despite their technical feasibility, the time needed to acquire a single 3D fast and turbo spin-echo MRI pulse sequence ranged between 15 and 20 minutes, which was prohibitively long for clinical practice.[3] However, recent technical innovations in 3D MRI accelerations enable clinically available high-quality isotropic 3D fast and turbo spin-echo MRI pulse sequences within 5 minutes and less, providing viable additions or alternatives to standard 2D fast and turbo spin-echo MRI protocols of the ankle.[15,16]

3D fast and turbo spin-echo MRI pulse sequences can be acquired with the same MRI scanners and the same MRI coils as 2D MRI without requiring specialized equipment or scanner technology. Either 1.5 Tesla (T) or 3.0 T MRI scanners can be used; however, 3D fast and turbo spin-echo MRI pulse sequences substantially benefit from the higher signal of 3.0 T MRI regarding acquisition speed, image resolution, and tissue contrast.[13]

Multiple studies evaluated the performance of 3D fast and turbo spin-echo MRI in the ankle, typically employing a combination of proton density- and T2-weighted contrasts.[3,15,16] Five-minute non-fat-suppressed proton density-weighted 3D data sets can be acquired with an isotropic voxel size of 0.5 x 0.5 × 0.5 mm^3, providing a good balance between acquisition times and high in-plane resolution with thin slices for the display of fine anatomic details (**Table 1**).[17–19] Five-minute fat-suppressed proton density-or T2-weighted 3D data sets can be acquired with an isotropic voxel size of 0.6 x 0.6 × 0.6 mm^3 providing exquisite fluid sensitivity for detecting subtle signal abnormalities (see **Table 1**).[3,17,18]

Since fat-suppressed and non-fat-suppressed MRI pulse sequences should always be used in conjunction, a practical 3D MRI protocol includes a pair of non-fat-suppressed proton density-weighted and fat-suppressed proton density-weighted or T2-weighted 3D fast or turbo spin-echo MRI pulse sequences for a whole-ankle MRI assessment. Clinically viable scenarios also include hybrid protocols which use a single 3D fast or turbo spin-echo MRI pulse sequence in combination with 2D fast or turbo spin-echo sequences. In our experience, a 10-min isotropic 3D fast or turbo spin-echo MRI protocol that includes a fat-suppressed fluid-sensitive 3D MRI sequence for detecting soft tissue edema, fluid collections, and bone marrow edema patterns, paired with a higher resolution non-fat-suppressed 3D fast and turbo spin-echo MRI for evaluating structural abnormalities, is a powerful combination for diagnosing a wide range of orthopedic or traumatic ankle conditions.[15,16,19]

This article provides an overview of the clinical application of 3D MRI of the ankle, reviews diagnostic performances of 2D and 3D MRI for diagnosing ankle abnormalities, and illustrates clinical 3D ankle MRI applications.

TECHNICAL ASPECTS OF 3D MRI IN CLINICAL PRACTICE

When considering the practical aspects of clinical implementation, several differences exist between 2D and 3D MRI of the ankle, which primarily apply to image acquisition and diagnostic interpretation techniques (see **Fig. 1**).

Table 1
3.0 T 3D CAIPIRINHA SPACE turbo spin echo protocol for ankle MRI

	3D MRI Protocol	
Parameters	**Proton Density-Weighted 3D CAIPIRINHA SPACE**	**T2-SPAIR 3D CAIPIRINHA SPACE**
Orientation	Sagittal	Sagittal
Repetition time [ms]	1000	1100
Echo time [ms]	28	110
Echo train length	54	42
Receiver bandwidth (Hertz/pixel)	422	399
Field-of-view [mm]	160 x 160	160 x 160
Voxel dimensions [mm]	0.5 x 0.5 x 0.5	0.63 x 0.63 x 0.63
Number of Slices	176	144
In-plane frequency encoding direction	Anterior-to-posterior	Anterior-to-posterior
Acquisition time	4 min 46 s	5 min 10 s

Abbreviations: CAIPIRINHA, Controlled Aliasing In Parallel Imaging Results IN higher acceleration; SPACE, sampling perfection with application optimized contrast using different flip angle evolutions; TSE, turbo spin echo.

2D and 3D MRI of the ankle are typically performed with the patient in a supine position and the foot placed in a dedicated boot-shaped foot-and-ankle coil designed to provide a comfortable position for the patient. For ankle MRI, the images typically extend from the distal tibia and fibula to the heel and the bases of the metatarsal bones in the sagittal, axial, and coronal planes.

3D pulse sequences of the ankle are usually acquired in the sagittal plane since this is typically the most time-efficient solution. Axial and coronal images are not acquired directly but are reformatted from the isotropic sagittal MR images after the exam has ended. The isotropic geometry of the voxels with the same length in all dimensions permits the reformation of any plane orientation from the parental sagittal data set without losing image quality. 2D MRI sequences do not allow useful secondary reformations and have to be acquired separately for any desired imaging plane.

The magic angle effect is a commonly encountered artifact around the angle, which primarily occurs in structures with tightly packed parallel bundled fibers of ligaments and tendons. On MR images of pulse sequences with a short echo time of up to approximately 50 ms, such as proton density- and T1-weighted MR images, it induces an artificial signal increase in structures oriented with an angle of 55° to the z-axis of the main magnetic field (B_0), which is typically the longitudinal direction of the MR scanner. In the ankle, the strongest magic angle effect can be found at the flexor and peroneal tendons at the level of the malleoli.[20] MRI sequences with a long echo time, such as T2-weighted pulse sequences, are least prone to the magic angle effect and represent a valuable part of clinical ankle MRI protocols (**Fig. 4**). Another practical possibility to eliminate the magic angle effect is to perform ankle MRI exams with patients in the prone position; however, the boot-shaped ankle coil may no longer be used then, but open coils, such as a knee surface coil. Prone patient positioning eliminates the magic angle artifact in the long flexor and peroneal tendons, as this ankle

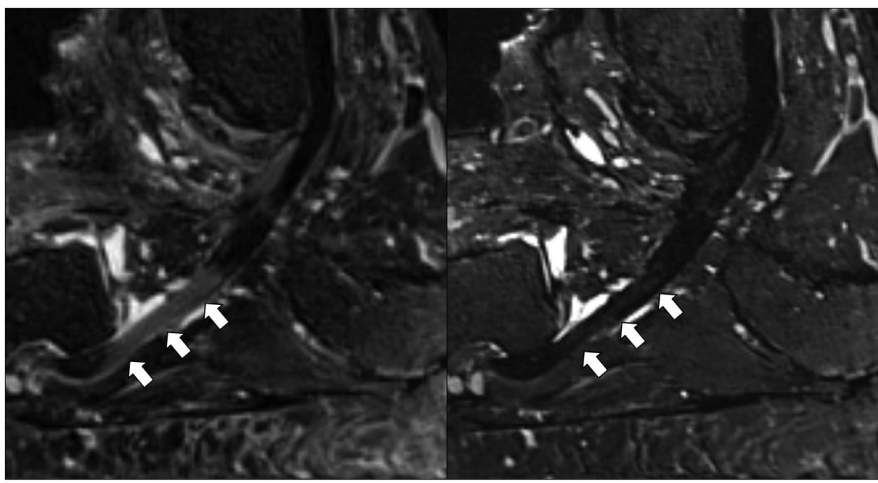

Fig. 4. Magic angle effect of the peroneus longus tendon. Fat-suppressed proton density-weighted and T2-weighted curved planar 3D reformation images of the peroneus longus tendon (*arrows*) demonstrate the magic angle effect characterized as an increased tendon signal (*arrows* in the *left image*) with a short echo time of 35 ms. The magic angle effect (*arrows* in the *right image*) is minimized with a longer echo time of 105 ms, indicated by normal low signal intensity of the tendon segement.

position results in an almost parallel course of the tendons to the z-direction of the static magnetic B0 field. However, it should be noted that the orientation of the prone position and plantar flexion alters the medial and lateral collateral ligament orientations, potentially obscuring small tears. Furthermore, some patients will find this position uncomfortable and may induce more motion artifacts.

MRI scanner field strength, such as 1.5 T versus 3.0 T, is a critical factor for achieving high 3D MRI image quality.[3,13] In principle, 3D MRI exams of the ankle may be obtained at 1.5 T and 3.0 T; however, 3.0 T MRI scanners yield approximately twice the signal compared to 1.5 T scanners, which can be translated into higher image quality and faster scanning. While 3D MRI of the ankle may be obtained at 1.5 T with lower image resolution or substantially longer scan times, most published studies have been performed at 3.0 T. To ensure high MRI exam quality, our preferred and recommended MRI scanner choice for 3D MRI of the ankle is 3.0 T with a dedicated boot-shaped foot and ankle surface coil.[3,15,16]

Modern 3D fast and turbo spin-echo ankle MRI pulse sequences have similar contrast characteristics as 2D fast and turbo spin-echo MR images[17,18]; however, the image texture may vary depending on the sequence type, slice thickness, contrast parameter settings, acceleration technique, manufacturer, and viewing software.[10,15,16] 3D fast and turbo spin-echo MR images often appear edge-enhanced, which may need some time to get used to.

Modern viewer software is required to efficiently review and take full advantage of the capabilities of 3D ankle MRI exams. Most modern enterprise-grade PACS systems include suitable viewer software. In addition, many capable standalone DICOM viewers are commercially available for personal and Apple computers. Key capabilities to take full advantage of isotropic 3D MRI data sets include interactive and dynamic multiplanar reformation modes, adjustable slice thicknesses, maximum and minimum intensity projections, linear and curved planar reformation functions (**Fig. 5**), and synchronized zoom, panning, and rotation of linked viewports. Creating thick-slap reformations dynamically with standard signal intensity averaging from

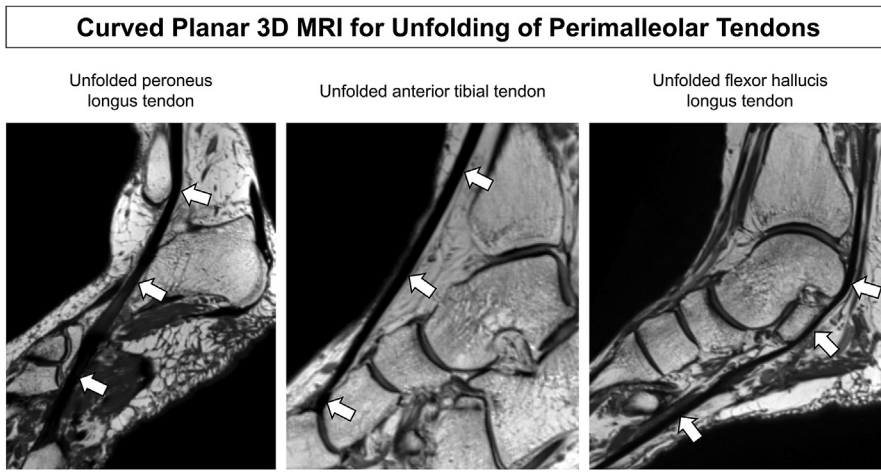

Fig. 5. 3D MRI unfolding of ankle tendons using curved planar reformation. Using a single multiaxial isotropic high-resolution 3D MRI dataset, dedicated curved multiplanar reformation images can be created for any curved tendon about the ankle. The unfolding reformation results in a planar long-axis display of double- and triple-angulated tendons (*arrows*), avoiding partial volume effects for better display and evaluation.

high-resolution isotropic thin-slice 3D fast and turbo spin-echo data sets can help reduce image noise and achieve a more 2D fast and turbo spin-echo-like image appearance, particularly for fat-suppressed data sets.[17,19,21] Reformating images with thicknesses of 1.0 to 1.5 mm may be a good balance between high-resolution thin-slice 3D MRI and 2D fast and turbo spin-echo-like image appearance for clinical interpretation.

3D MRI can also improve scan efficiency, thereby shortening ankle MRI examinations.[3,15,16] Several studies have shown that using a single 3D fast or turbo spin-echo MRI sequence instead of two or three standard 2D fast or turbo spin-echo sequences within an ankle MRI exam can shorten the total scan time.[15,16,22–24] Clinically available, modern acceleration techniques result in high-quality 3D fast and turbo spin-echo sequences in under 5 minutes,[3,10,17,18,25] saving up to 50% of the time compared to 2D fast and turbo spin-echo sequences with acquisition times of around 3 minutes each. Recent advances in artificial intelligence-based image reconstruction have substantially reduced 2D and 3D MRI scan times.[6,10,25] The time-saving potentials of 2D and 3D MRI evolve rapidly and will depend on locally available MRI sequences, surface coils, and MRI scanners.

TECHNICAL PERFORMANCE OF 3D MRI

In recent years, several studies have been conducted to compare technical image characteristics of 3D fast and turbo spin-echo MRI sequences with their 2D counterparts.[3] These studies have demonstrated that 3D fast and turbo spin-echo MRI can create comparable image signal strength (signal-to-noise ratios) and tissue contrast (contrast-to-noise ratios) and depicts anatomical structures at least as well as 2D fast and turbo spin-echo MRI.

The first results of a spin-echo-based 3D MRI sequence for the ankle were published in 2008.[22] The study found that T2-weighted 3D fast spin-echo MRI with and without fat suppression had significantly higher image signal strength than 2D fast spin-echo MRI and comparable image tissue contrast. Although image quality was judged similarly between the 2D and 3D fast spin-echo MRI exams, 3D MRI showed more blurring. The scan time for the 3D ankle MRI sequence was 5 to 6 minutes with isotropic voxels of 0.6 mm edge length.

In 2012, another 3D ankle MRI study evaluated a T2-weighted 3D turbo spin-echo MRI sequence with fat suppression.[23] 3D MRI had significantly higher image signal strength and contrast for fluid and articular cartilage than 2D turbo spin-echo MRI sequences. 3D MRI was superior for depicting articular cartilage, collateral ligaments, and the spring ligament complex.

Over the past 15 years, multiple 3.0 T studies have shown that 3D fast and turbo spin-echo MRI sequences create comparable image signal strength and contrast and depict anatomic joint structures and tissues at least, as well as 2D fast and turbo spin-echo MRI.

In 2016, a novel 4-fold accelerated 3D turbo spin-echo MRI sequence called CAIPIRINHA SPACE was introduced for 3D ankle MRI.[15] The pulse sequence was initially developed for the knee[19,21] and later adopted for the ankle.[15,16] Advantageous features included a novel bidirectional 2 x 2 parallel imaging acceleration pattern, which increases signal gain compared to older techniques.[10,13,25] 3D CAIPIRINHA SPACE MRI creates similar image characteristics to corresponding 2D MR images. The faster acceleration permits proton density-weighted 3D MRI with a voxel size of 0.5 x 0.5 $\times$ 0.5 mm^3 and fat-suppressed T2-weighted 3D MRI with a voxel size of 0.6 x 0.6 $\times$ 0.6 mm^3 at around 5 min scan time for each. 3D CAIPIRINHA SPACE MRI is

our favorite technique for daily clinical practice and our recommended technique for 3D ankle MRI.

Ankle Ligaments

Ankle ligaments are important stabilizers of the syndesmosis and talocrural, subtalar, and midfoot joints. On MRI, normal ligaments appear with low signal intensity on T1-weighted, proton density-weighted, and T2-weighted MR images regardless of fat suppression. However, some ligaments have naturally occurring fatty striations interposed between intact ligament strands, appearing as alternating "zebra-like" linear bright and dark signal intensities on nonfat-suppressed high-resolution MR images (**Fig. 6**).

Ligament injuries range from low-grade interstitial injuries to complete retracted and displaced tears (**Table 2**) (**Fig. 7**). Low-grade interstitial ligamentous injuries present with edematous interstitial signal intensity on fluid-sensitive proton density-weighted and T2-weighted MR images. Due to their fluid insensitivity, the edematous signal abnormalities are typically not visible on T1-weighted MR images. In addition to the edematous signal, the injured ligaments may appear enlarged but without visible disrupted fibers. Partial-thickness tears show clearly defined disrupted and continuous fibers. The term "high-grade partial-thickness tear" is not clearly defined but might be most often applied to indicate greater than 50% fiber disruption of the cross-sectional ligament area. Full-thickness tears require the disruption of all ligament fibers. Fluid-filled gap formation indicates fiber retraction. Similar to a classic Stener

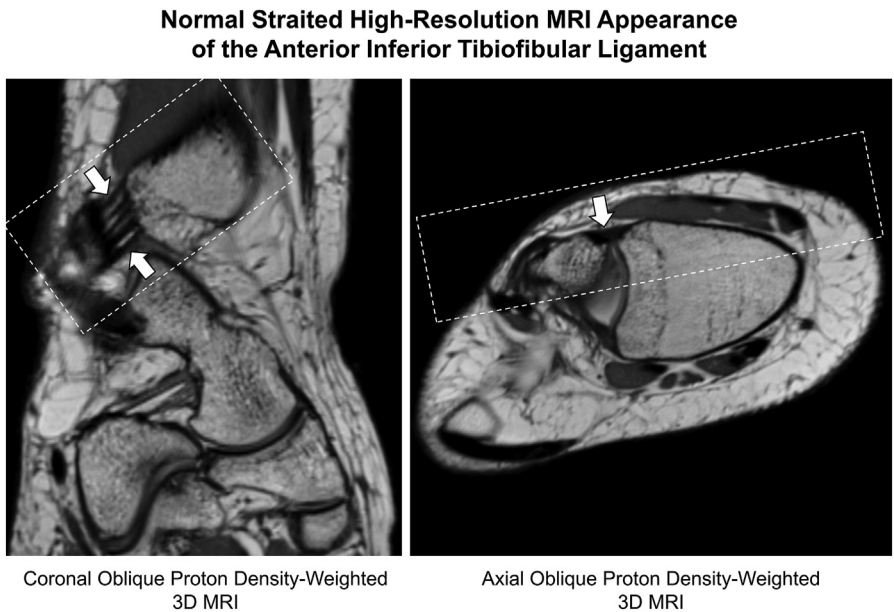

Fig. 6. High-resolution 3D MRI appearance of striated ligaments. Coronal oblique (*left image*) and axial oblique (*right image*) program density-weighted 3D MRI reformation images demonstrate the normal striated appearance of the anterior talofibular ligament of the syndesmosis on the coronal oblique 3D MR image (*arrows* in *left image*). Upon anatomic alignment along the course of the ligament on the axial oblique 3D MR image, the ligament fibers appear continuous and with intact hypointense MRI signal (*arrow* in the *right image*). The dashed boxes indicate the slice orientations.

Table 2
MRI terminology and MRI findings of ligamentous injuries

Ligament Integrity and MRI Terminology	MRI Findings
Interstitial injury	Increased proton density and T2 signal inside the ligament without visualized fiber disruption
Partial-thickness tear	Mixed disrupted and intact ligament fibers
Full-thickness tear	Disruption of all ligament fibers with optional fiber retraction and displacement of torn ligament ends.

lesion in the thumb ulnar collateral ligament and knee medial collateral ligament,[2,26] torn ligament ends may displace, such as the calcaneofibular ligament, on top of the overlying peroneal tendons.

Lateral Collateral Ligaments

The lateral collateral ligaments are the most frequently injured ankle ligaments and are involved in about 60% to 80% of all ankle injuries.[27,28] Inversion trauma is the most common mechanism of injury. The anterior tibiofibular ligament (ATFL) is most commonly injured (see **Fig. 7**; **Fig. 8**), followed by the calcaneofibular ligament (CFL) and rarely the posterior tibiofibular ligament (PTFL).

Scarring and remodeling of the lateral collateral ligaments are common MRI findings in the general population, usually indicating healed ligament trauma, which may ormay not corroborate a clinical diagnosis of chronic lateral ankle instability. The spectrum of scar-remodeled lateral collateral ligaments includes thinner and thicker than normal ligament diameters, irregular ligament surfaces, and higher than normal, non-edematous signal intensities on proton density-weighted, T2-weighted, and also T1-weighted MR images, which reduces to normal with increasing maturation of healing.

In 2D MRI, axial and coronal plane images are typically used to evaluate the lateral collateral ligaments. However, as the ATFL has an axial oblique and the CFL has a coronal oblique course, they are typically not visible in profile on a single standard axial,

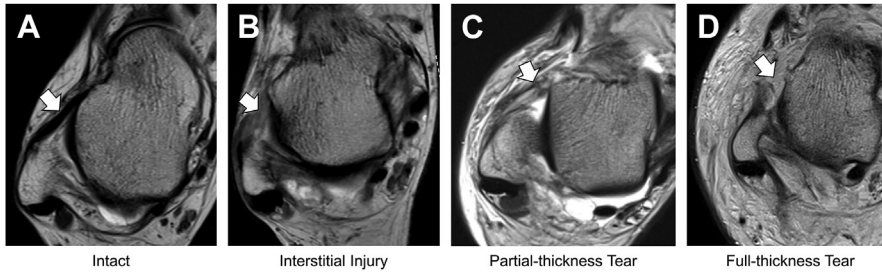

Fig. 7. MRI appearances of ligament integrity. Axial proton density-weighted MR images show the spectrum from intact (*A*) to full-thickness tear (*D*) of the anterior talofibular ligament (*arrows*). (*A*) Intact ligaments appear taut, dark, and sharply demarcated (*arrow*). (*B*) Interstitial ligament injuries appear with increased internal edema-like protein density or T2 signal and optional thickening (*arrow*), but no discrete fiber disruption. (*C*) Partial-thickness ligament tears show mixed discontinuous and continuous ligament fibers (*arrow*). (*D*) Full-thickness anterior talofibular ligament tears show the disruption of all ligament fibers (*arrow*) and often a fluid-filled gap.

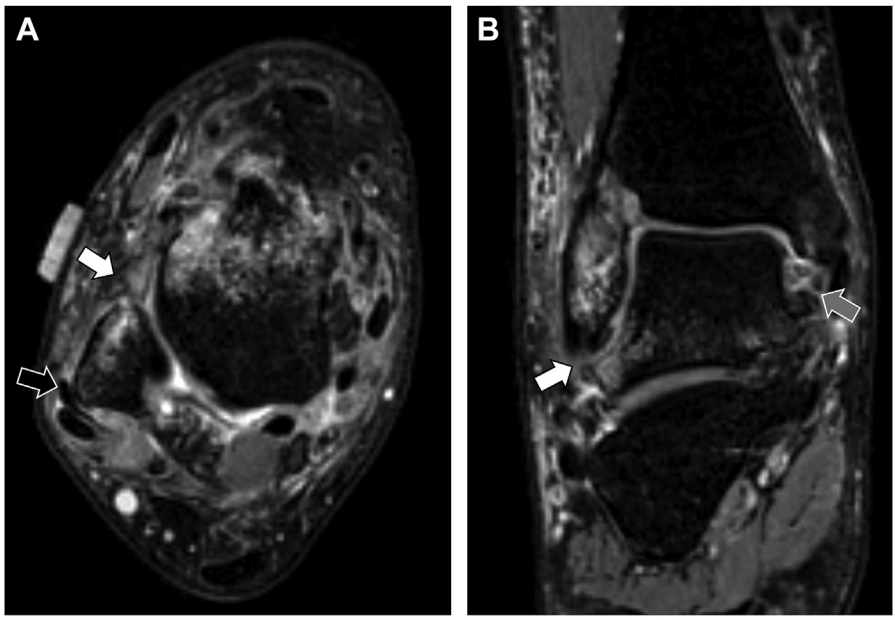

Fig. 8. 3D MRI after ankle trauma in a 16-year-old teenager. Axial (*A*) and coronal (*B*) T2-weighted fat-suppressed 3D MRI reformations show a full-thickness anterior talofibular ligament tear (*white arrows* in *A* and *B*), full-thickness deltoid ligament complex tear (*gray arrows* in *B*), and laterally subluxated peroneal tendons (*black arrow* in *A*) due to tearing of the superior peroneal retinaculum retinaculum.

sagittal, or coronal 2D MR image but cut obliquely through multiple slices. Acquiring dedicated 2D MR images aligned individually to oblique ligaments is possible but time-consuming (see **Fig. 6**). The limitless multiplanar reformation capabilities of 3D MRI enable the alignment of long and short-axis images to oblique ligaments individually and interactively during readout.

Overall, the reported diagnostic accuracy of MRI for diagnosing ATFL tears is high, with reported sensitivities of 80%–100% and specificities of up to 100%.[29,30] Several studies showed similar diagnostic performances of 2D and 3D fast and turbo spin echo MRI techniques for detecting lateral collateral ligament injuries.[16,23,31,32] A study of 101 clinical patients found that T2-weighted 3D turbo spin echo MRI had a higher sensitivity of 96% versus 84% to 86% of 2D turbo spin echo MRI for detecting ATFL injuries.[24] The specificities were similar between 2D and 3D MRI, whereas 3D MRI had superior edge sharpness. Another study comparing 2D and 3D turbo spin echo MRI techniques found a statistically similar diagnostic performance for detecting CFL injuries, although the 3D MRI image quality was considered inferior.[33]

An anatomical morphology study applying 3D turbo spin echo MRI described a double-bundled appearance of the ATFL, with tearing of both bundles as the most common pattern in acute ankle sprains.[34] Another study evaluating the obliquely oriented CFL and peroneus tendon relationship found that the peroneal muscle-tendon unit act as a fulcrum for the deeper positioned CFL, which had a significantly lower angulation in maximum plantar flexion than in the neutral position.[35]

Medial Collateral Ligament Complex and Spring Ligament

The deltoid ligament complex, also known as the medial collateral ligament complex, comprises a superficial and deep layer. The superficial layer includes the talonavicular, tibiospring, and talocalcaneal ligaments, whereas the deep layer includes the anterior and posterior tibiotalar ligaments. Unlike lateral collateral ligament injuries, medial collateral ligament injuries are less common, accounting for only 10% to 16% of ankle injuries in athletes.[36,37] High-energy trauma with forced ankle eversion is the most commonly reported mechanism of injury. Medial collateral ligament tears often occur with lateral collateral and syndesmotic ligament injuries. MRI detects and characterizes medial collateral ligament injuries with 84% to 100% sensitivity and 93% to 100% specificity.[38,39]

The spring ligament complex comprises three parts that stabilize the medial arch connecting the calcaneus and navicular bones, including the superomedial, medioplantar oblique, and inferoplantar longitudinal components.[40] Full-thickness tearing of the spring ligament complex is rare. Still, remodeling with chronic scarring, waviness, and elongation are common MRI findings after ankle sprains with concomitant midfoot and peritalar translation injuries.

With 2D MRI, the coronal plane is typically used to evaluate the medial collateral ligament complex and superomedial spring ligament. In contrast, the plantar spring ligaments are typically evaluated on axial and sagittal plane MR images. However, partial volume effects secondary to thick slice thickness and oblique ligament orientations can result in incomplete visualization on standard 2D MR images. The limitless multiplanar reformation capabilities and much thinner slice thickness of 3D MRI data sets permit the individual alignment of imaging planes to visualize the medial collateral (see **Fig. 8**) and spring ligaments better.

Two studies compared the diagnostic performance of 2D turbo spin echo and 3D SPACE turbo spin echo MRI for detecting medial collateral and spring ligament injuries after acute ankle injuries.[16,23] The first study published in 2012 found no significant differences in detecting medial collateral ligament tears comparing axial, sagittal, and coronal fat-suppressed T2-weighted sequence with a single isotropic fat-suppressed T2-weighted 3D SPACE turbo spin echo sequence.[23] However, the other study published in 2016 found significantly more ligament tears with 3D than 2D MRI using a modern comprehensive 10-min whole-ankle 3D CAIPIRINHA SPACE MRI protocol, comprised of isotropic proton density-weighted and an isotropic fat-suppressed T2-weighted 3D MRI data sets.[16]

Syndesmosis

The syndesmosis is the primary stabilizer of the distal tibiofibular joint. The syndesmosis typically includes the anterior inferior tibiofibular ligament (see **Fig. 6**), the posterior inferior tibiofibular ligament, the interosseous ligament, and the interosseous membrane.

Multiple injury mechanisms may cause syndesmotic injuries, but the most common injury mechanism comprises dorsiflexion with external rotation on a planted foot.[41] Syndesmotic injuries occur with a 10% to 17% incidence.[42,43] Diagnosing syndesmotic injuries can be challenging, but it is crucial to prevent instability.[44–46] Treatment options range from immobilization to surgical repair and reconstruction.[5,47]

2D MRI has a 97% accuracy for detecting anterior and 100% accuracy for detecting posterior inferior tibiofibular ligaments.[48] As the syndesmotic ligaments have an oblique axial course, 45-degree angulated axial oblique 2D MR images may be obtained to improve tear detection. However, the multiplanar reformation capabilities of 3D MRI permit individual plane alignment along the syndesmotic ligament fibers for accurately detecting acute and chronic syndesmotic injuries (see **Fig. 6**; **Fig. 9**).[49] A 2017 study

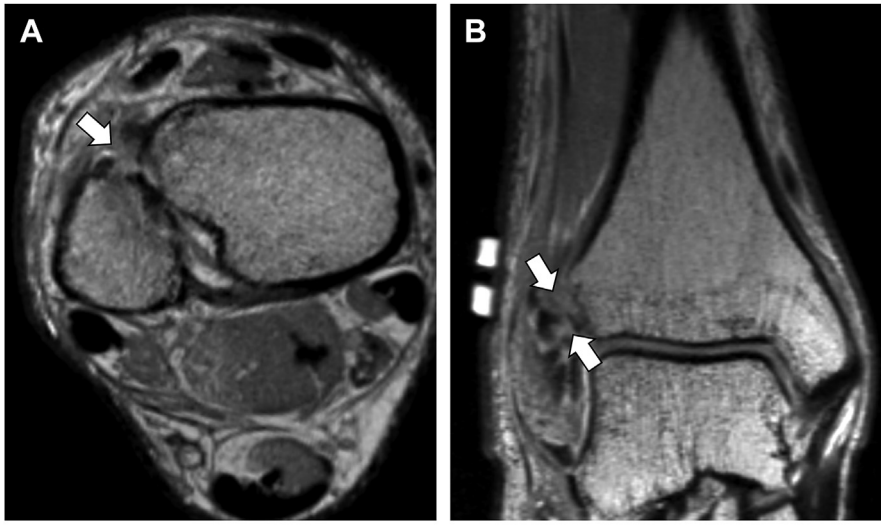

Fig. 9. 3D MRI after ankle trauma in a 29-year-old man. Oblique axial (*A*) and oblique coronal (*B*) proton density-weighted 3D MRI reformations show a full-thickness anterior tibiofibular ligament tear (*arrows*).

found similar accuracies in detecting anterior inferior and posterior inferior tibiofibular ligament tears using axial oblique T2-weighted 2D and proton density-weighted 3D turbo spin echo SPACE MRI reformation images, with accuracies ranging from 96% to 100%.[50]

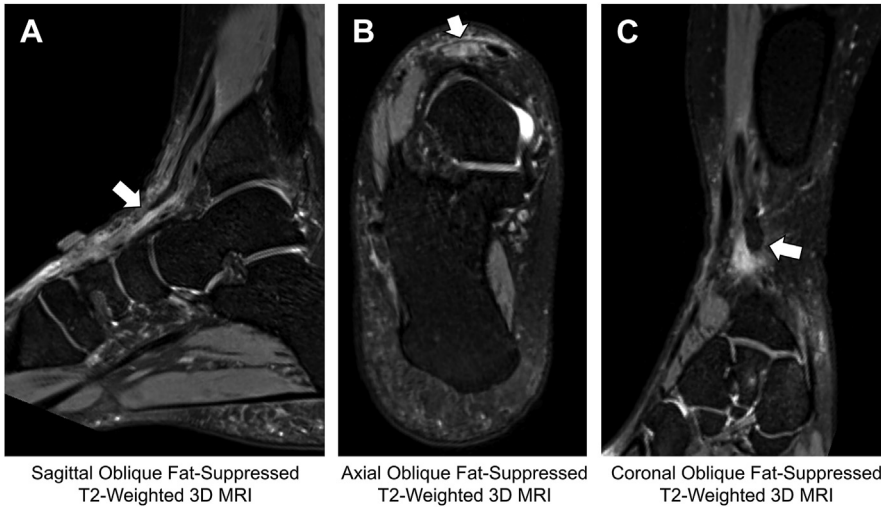

Fig. 10. 3D MRI after ankle trauma in a 44-year-old woman. Oblique sagittal (*A*), the axial (*B*), and oblique coronal (*C*) fat-suppressed T2-weighted MRI reformation images demonstrate a 6 cm retracted extensor hallucis longus tear. The proximally retracted tendon is located at the talonavicular joint line (*white arrows* in *A* and *C*). The axial oblique MRI reformation image (*B*) distal to the retracted tendon demonstrates an empty tendon sheath (*arrow* in *B*).

Tendons

The hindfoot tendons include the extensor, flexor, peroneal, and Achilles tendons and plantar fascia. In concert, the hindfoot tendons act as joint and arch stabilizers and facilitate complex ankle movements such as inversion, eversion, plantarflexion, and dorsiflexion. For example, the posterior tibial tendon is the primary dynamic stabilizer of the medial longitudinal arch, and degeneration or dysfunction can lead to an adult-acquired flatfoot deformity and progressive collapsing foot deformity.[51,52] Ankle pain may be caused by degenerative tendinopathy, tenosynovitis, and traumatic tears, but tendon abnormalities may also be asymptomatic, particularly peroneal tendon tears[53] .[54] Traumatic injuries of the tendons are much less common than ligament injuries, occurring in up to 3% of acute ankle injuries.[28,55]

Due to the complex multidirectional course of the hindfoot tendons, multiple MR imaging planes are necessary to visualize the different tendon portions appropriately. Separately acquired axial and sagittal oblique 2D MRI sequences with perpendicular orientation to the long axis of the flexor and peroneal tendons may be obtained at the medial and lateral malleolus level to improve the visualization of the different tendon

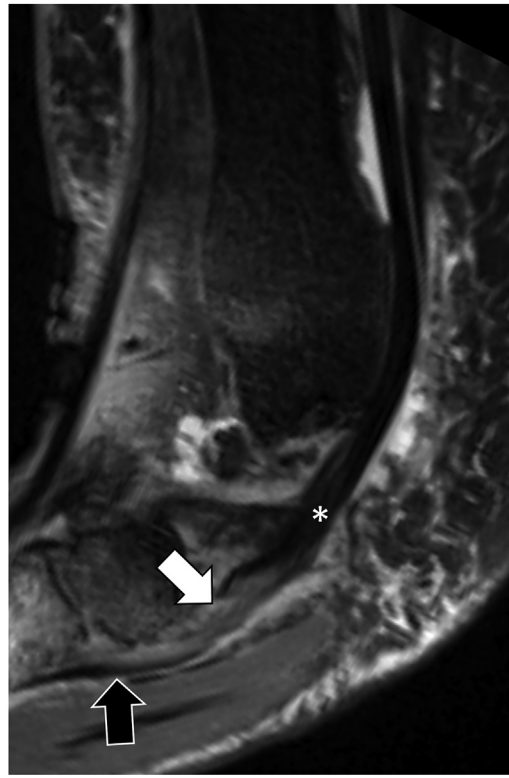

Fig. 11. 3D MRI of the ankle in a 58-year-old woman with chronic ankle pain. Curved planar fat-suppressed T2-weighted 3D MRI reformation image along the posterior tibial tendon (*asterisk*) shows a mildly retracted full-thickness navicular attachment tear (*white arrow*) and continuous plantar attachment fibers (*black arrow*).

segments but substantially prolong acquisition times. The multiplanar reformation capabilities of 3D MRI also include a mode called "curved planar reformation," which allows the "unfolding" of multidirectional structures, such as the extensor (Fig. 10), long flexor (Fig. 11), and peroneal (Figs. 12 and 13) tendons, into a single image plane (see Fig. 5).

The magic angle effect poses a clinically relevant challenge for 2D and 3D MRI of ankle tendons. The long flexor and peroneal tendons are especially prone to abnormally high signal intensity due to the magic angle effects around the medial and lateral malleolus. To eliminate magic angle effects, 3D MRI sequences with long echo times may be included in ankle MRI protocols, such as a T2-weighted 3D turbo spin echo MRI sequence without or with fat suppression (see Fig. 4). However since magic angle effects occur predictably typically affected tendon segments should be evaluated based on morphology rather than signal intensity on sequences with short echo times.

A 2019 study found around the ankle reduced magic angle effects and improved the visualization of tendons with isotropic proton density-weighted and fat-suppressed T2-weighted 3D CAIPIRINHA SPACE turbo spin echo MRI sequences.[16] Another study also applied proton density-weighted and fat-suppressed T2-weighted 3D CAIPIRINHA SPACE MRI and found improved tendon visualization and similar diagnostic performance for the detection of tears compared to a similar 2D ankle MRI protocol.[23]

Articular Cartilage

MRI has high accuracy for detecting talocrural, subtalar, talonavicular, and tarsometatarsal articular cartilage lesions, including articular cartilage defects, osteochondral lesions, chondral and osteochondral sheer injuries, and fractures (Table 3).[5] Osteochondral lesions are characterized by loss of cartilage integrity with or without subchondral bone fragments (Table 4).[56] Osteochondral lesions are commonly traumatic, in which MRI provides high accuracy for detection and predicting stability.[57,58]

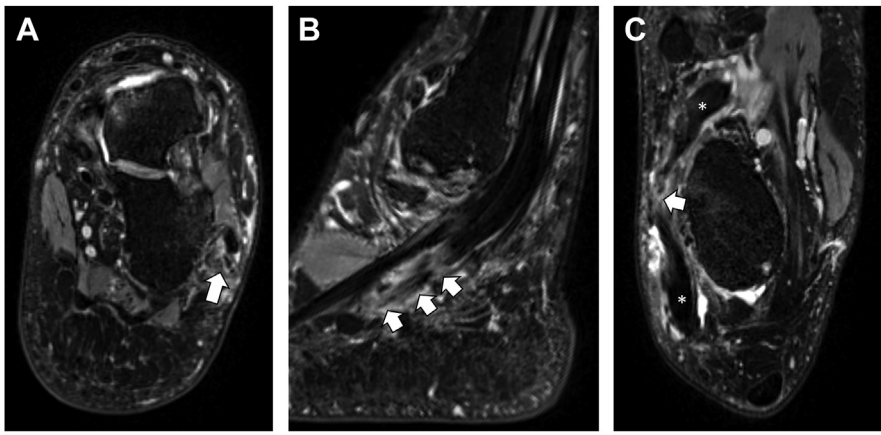

Fig. 12. 3D MRI of the ankle in a 57-year-old man with chronic lateral ankle pain. Oblique axial (*A*), oblique sagittal (*B*), and oblique coronal (*C*) fat-suppressed T2-weighted MRI reformation images demonstrate a full-thickness peroneus longus tear (*white arrows*) with retracted proximal and distal tendon ends (*asterisks* in *C*).

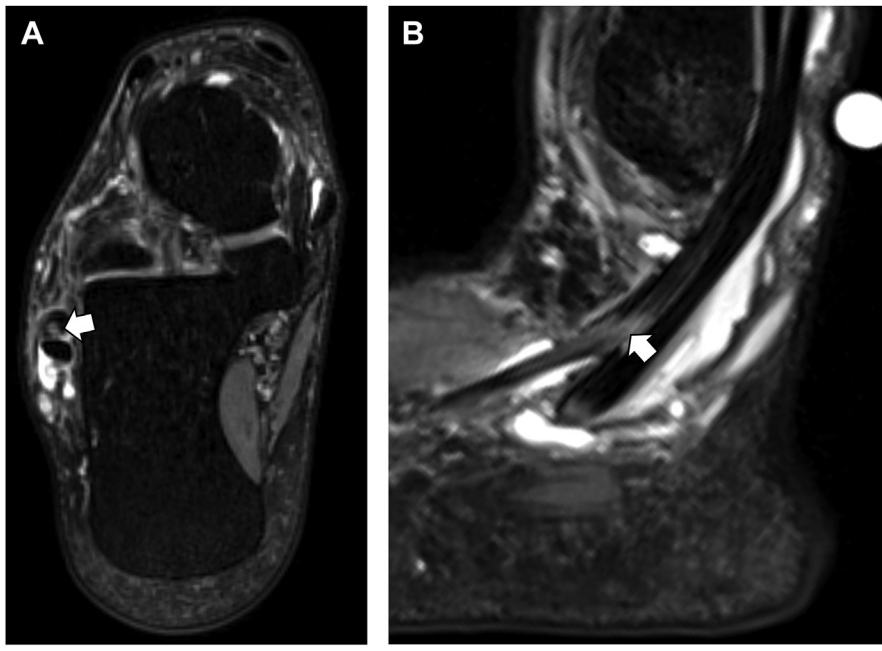

Fig. 13. 3D MRI of the ankle in a 37-year-old man with chronic lateral ankle pain. Oblique axial (*A*) and oblique sagittal (*B*) fat-suppressed T2-weighted MRI reformation images demonstrate a partial longitudinal peroneus brevis split tear (*arrows* in *A* and *B*).

Fluid-sensitive MRI pulse sequences with high spatial and contrast resolution help detect small osteochondral lesions and characterize cartilage integrity. Proton density-weighted fast, and turbo spin echo MRI pulse sequences provide the best contrast for articular cartilage evaluation. However, curved articular cartilage surfaces can create blind spots on 2D MRI, which 3D MRI overcomes (Fig. 14). Unlike 2D MRI,

Table 3
Types of osteochondral injuries

Type	MRI Appearance
Bone contusion	Focal bone marrow edema pattern. Absent cortical contour deformity. Absent fracture lines. The overlying cartilage is structurally intact.
Subchondral fracture	Focal bone marrow edema pattern. Absent cortical contour deformity. Subcortically located fracture line that parallels the articular surface. The overlying cartilage is structurally intact.
Osteochondral fracture	Focal bone marrow edema pattern. Typically presents with contour deformities, articular surface step-off, or displaced fragments. The fracture line extends through bone and articular cartilage.
Chondral fracture	Focal bone marrow edema pattern. Presents with articular cartilage contour irregularities. The separation typically occurs at the calcified-noncalcified cartilage interface near the tidemark layer. Chondral fragments may remain in situ or float in the joint cavity.

Table 4
MRI classification of osteochondral lesions of the talus

Grade	Description
1	Normal
2	Partial-thickness articular cartilage defect
3	Coapted full-thickness articular cartilage defect or exposed bone
4	Unstable but non-displaced in-situ chondral or osteochondral fragment
5	Displaced chondral or osteochondral fragment

cartilage-sensitive 3D MRI, including fast and turbo spin echo and 3D gradient-echo pulse sequences such as DESS, permits gapless thin section articular cartilage volume acquisitions for volumetry, mapping, and characterization of articular cartilage lesions.[4]

MRI has a high accuracy for detecting cartilage defects in the ankle, specifically in the talocrural joint.[59,60] Studies have shown a similar or better performance of qualitative or quantitative articular cartilage assessments with 3D than 2D fast and turbo spin echo sequences.[15,16,22,23,32,61] Fluid-sensitive MRI pulse sequences with high spatial and contrast resolution are beneficial in detecting small osteochondral lesions and characterizing cartilage integrity. A 2019 study validated the application of 3D fast and turbo spin echo MRI for detecting osteochondral lesions of the talar dome and tibial plafond. Proton density-weighted 3D MRI sequences with and without compressed sensing acceleration showed good-to-very good performance for detecting osteochondral lesions.[18,31]

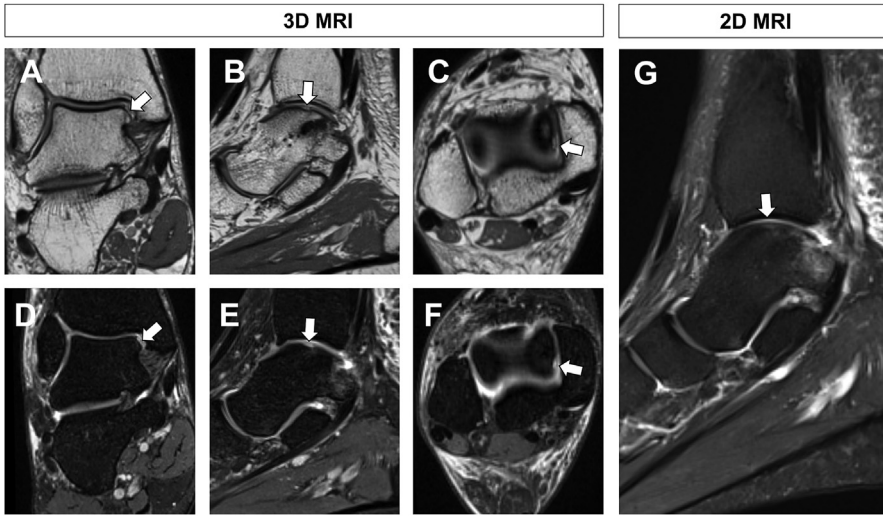

Fig. 14. 3D and 2D MRI of the ankle in a patient with recalcitrant ankle pain after trauma. Oblique coronal (*A* and *D*), oblique sagittal (*B* and *E*), and oblique axial (*C* and *F*) proton density-weighted (*A–C*) and fat-suppressed T2-weighted (*D-F*) 3D MRI reformation images demonstrate an osteochondral lesion of the medial talar dome with full-thickness articular cartilage loss and mild convex deformity of the exposed subchondral plate (*white arrows* in *A–F*). Note that on the fat-suppressed T2-weighted 2D MR image (*G*), the lesion is partially obscured and underestimated (*arrow*) due to partial volume effects.

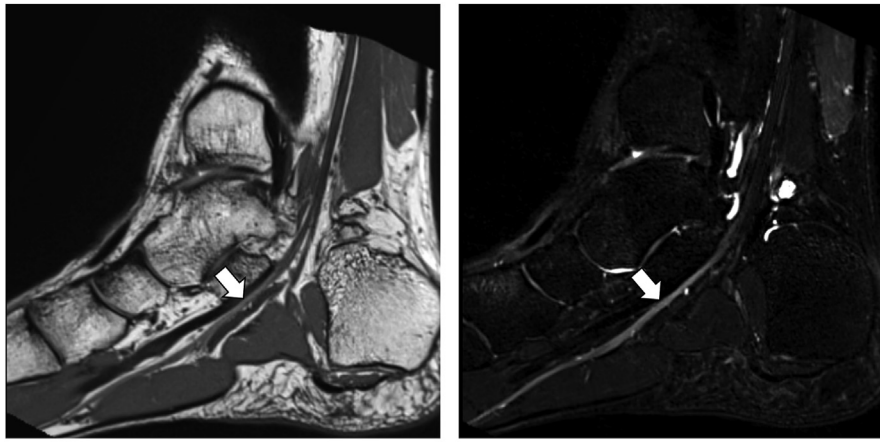

Fig. 15. 3D MRI of medial plantar neuropathy. Curved planar reformation images along the course of the medial plantar nerves (*arrows*) of proto-density-weighted (*left image*) and fat-suppressed T2-weighted (*right image*) MR images demonstrate a thickened and edematous medial plantar nerves (*arrows*) indicating neuropathy. The fat-suppressed T2-weighted 3D MR image was acquired with an echo time greater than 100 ms to eliminate magic angle effects.

Other Structures

Multiple studies applying 3D MRI in evaluating various conditions and structures of the ankle highlight a broad range of applications, taking advantage of the isotropic voxel dimensions and thin section capabilities of 3D MRI.

A 2012 study compared the visibility of the Lisfranc ligaments of fat-suppressed isotropic proton density-weighted 3D SPACE MRI and axial, sagittal, and coronal fat-suppressed proton density-weighted 2D turbo spin echo MRI.[62] The multiplanar reformation and thin section capabilities of 3D MRI depicted the delicate Lisfranc ligament fibers to better advantage than 2D MRI.

Another study employing T2-weighted 3D fast and turbo spin echo MRI for evaluating the subtalar and sinus tarsi ligaments in patients with subtalar instability suggested that the thinning of the anterior capsular ligament may indicate subtalar instability.[63]

A study evaluating the value of 3D MRI in diagnosing anterolateral ankle impingement found higher sensitivity and specificity for contrast-enhanced T1-weighted 3D gradient-echo MRI than 2D MRI.[64]

A study applying 3D gradient-echo MRI to visualize the tibial nerve along its course through the tarsal tunnel found 3D MRI advantageous for visualizing the tibial nerve bifurcations and branches may aid in avoiding nerve injury during surgery.[65] 3D MRI is exquisitely well suited to map the tibial and plantar nerves (**Fig. 15**).

SUMMARY

3D fast and turbo spin echo MRI is a newer, clinically available multiaxial MRI technique that improves the visualization of oblique and curved ligaments, tendons, and nerves around the ankle. Multiple studies have validated the accuracy of 3D MRI.

Clinical 3D MRI of the ankle can be acquired with 0.5 mm slice thickness to resolve small anatomic structures and abnormalities, such as tendon and ligament tears, osteochondral lesions, and nerve lesions. We recommend adding 3D MRI pulse sequences to traditional 2D MRI protocols to visualize small and curved ankle structures to better advantage.

CLINICS CARE POINTS

- 3D MRI is clinically available by multiple vendors and has been validated for use in clinical practice.
- Multiplanar 3D MRI reformation postprocessing for individual image plane alignment obliquely oriented ligaments can improve the detection and characterization of ligament tears.
- The high spatial thin section resolution of 3D MRI can improve the detection, characterization, and morphological grading of osteochondral lesions.
- Curved planar 3D MRI reformation for unfolding multidirectional tendons into one image plane can improve the detection and characterization of tendon degeneration and tears.

REFERENCES

1. Fong DT, Hong Y, Chan LK, et al. A systematic review on ankle injury and ankle sprain in sports. Sports Med 2007;37(1):73–94.
2. Fritz B, Fritz J. MR Imaging of Acute Knee Injuries: Systematic Evaluation and Reporting. Radiol Clin North Am 2023;61(2):261–80.
3. Fritz B, Fritz J, Sutter R. 3D MRI of the Ankle: A Concise State-of-the-Art Review. Semin Musculoskelet Radiol 2021;25(3):514–26.
4.. Walter SS, Fritz B, Kijowski R, et al. 2D versus 3D MRI of osteoarthritis in clinical practice and research. Skeletal Radiol 2023. https://doi.org/10.1007/s00256-023-04309-4.
5. Umans H, Cerezal L, Linklater J, et al. Postoperative MRI of the Ankle and Foot. Magn Reson Imaging Clin N Am 2022;30(4):733–55.
6. Lin DJ, Walter SS, Fritz J. Artificial Intelligence-Driven Ultra-Fast Superresolution MRI: 10-Fold Accelerated Musculoskeletal Turbo Spin Echo MRI Within Reach. Invest Radiol 2023;58(1):28–42.
7. Fritz J, Kijowski R, Recht MP. Artificial intelligence in musculoskeletal imaging: a perspective on value propositions, clinical use, and obstacles. Skeletal Radiol 2022;51(2):239–43.
8. Del Grande F, Rashidi A, Luna R, et al. Five-Minute Five-Sequence Knee MRI Using Combined Simultaneous Multislice and Parallel Imaging Acceleration: Comparison with 10-Minute Parallel Imaging Knee MRI. Radiology 2021;299(3):635–46.
9. Del Grande F, Guggenberger R, Fritz J. Rapid Musculoskeletal MRI in 2021: Value and Optimized Use of Widely Accessible Techniques. AJR Am J Roentgenol 2021;216(3):704–17.
10. Fritz J, Guggenberger R, Del Grande F. Rapid Musculoskeletal MRI in 2021: Clinical Application of Advanced Accelerated Techniques. AJR Am J Roentgenol 2021;216(3):718–33.
11. Fritz J, Fritz B, Zhang J, et al. Simultaneous Multislice Accelerated Turbo Spin Echo Magnetic Resonance Imaging: Comparison and Combination With In-

Plane Parallel Imaging Acceleration for High-Resolution Magnetic Resonance Imaging of the Knee. Invest Radiol 2017;52(9):529–37.
12. Park EH, de Cesar Netto C, Fritz J. MRI in Acute Ankle Sprains: Should We Be More Aggressive with Indications? Foot Ankle Clin 2023;28(2):231–64.
13. Khodarahmi I, Fritz J. The Value of 3 Tesla Field Strength for Musculoskeletal Magnetic Resonance Imaging. Invest Radiol 2021;56(11):749–63.
14. Mugler JP 3rd. Optimized three-dimensional fast-spin-echo MRI. J Magn Reson Imaging 2014;39(4):745–67.
15. Kalia V, Fritz B, Johnson R, et al. CAIPIRINHA accelerated SPACE enables 10-min isotropic 3D TSE MRI of the ankle for optimized visualization of curved and oblique ligaments and tendons. Eur Radiol 2017;27(9):3652–61.
16. Fritz B, Bensler S, Thawait GK, et al. CAIPIRINHA-accelerated 10-min 3D TSE MRI of the ankle for the diagnosis of painful ankle conditions: Performance evaluation in 70 patients. Eur Radiol 2019;29(2):609–19.
17. Fritz J, Fritz B, Thawait GG, et al. Three-Dimensional CAIPIRINHA SPACE TSE for 5-Minute High-Resolution MRI of the Knee. Invest Radiol 2016;51(10):609–17.
18. Fritz J, Raithel E, Thawait GK, et al. Six-Fold Acceleration of High-Spatial Resolution 3D SPACE MRI of the Knee Through Incoherent k-Space Undersampling and Iterative Reconstruction-First Experience. Invest Radiol 2016;51(6):400–9.
19. Del Grande F, Delcogliano M, Guglielmi R, et al. Fully Automated 10-Minute 3D CAIPIRINHA SPACE TSE MRI of the Knee in Adults: A Multicenter, Multireader, Multifield-Strength Validation Study. Invest Radiol 2018;53(11):689–97.
20. Fritz B, Fritz J. MR Imaging-Ultrasonography Correlation of Acute and Chronic Foot and Ankle Conditions. Magn Reson Imaging Clin N Am 2023;31(2):321–35.
21. Fritz J, Ahlawat S, Fritz B, et al. 10-Min 3D Turbo Spin Echo MRI of the Knee in Children: Arthroscopy-Validated Accuracy for the Diagnosis of Internal Derangement. J Magn Reson Imaging 2019;49(7):e139–51.
22. Stevens KJ, Busse RF, Han E, et al. Ankle: isotropic MR imaging with 3D-FSE-cube–initial experience in healthy volunteers. Radiology 2008;249(3):1026–33.
23. Notohamiprodjo M, Kuschel B, Horng A, et al. 3D-MRI of the ankle with optimized 3D-SPACE. Invest Radiol 2012;47(4):231–9.
24. Park HJ, Lee SY, Park NH, et al. Three-dimensional isotropic T2-weighted fast spin-echo (VISTA) ankle MRI versus two-dimensional fast spin-echo T2-weighted sequences for the evaluation of anterior talofibular ligament injury. Clin Radiol 2016;71(4):349–55.
25. Kijowski R, Fritz J. Emerging Technology in Musculoskeletal MRI and CT. Radiology 2023;306(1):6–19.
26. Rashidi A, Haj-Mirzaian A, Dalili D, et al. Evidence-based use of clinical examination, ultrasonography, and MRI for diagnosing ulnar collateral ligament tears of the metacarpophalangeal joint of the thumb: systematic review and meta-analysis. Eur Radiol 2021;31(8):5699–712.
27. Holmer P, Sondergaard L, Konradsen L, et al. Epidemiology of sprains in the lateral ankle and foot. Foot Ankle Int 1994;15(2):72–4.
28. Roemer FW, Jomaah N, Niu J, et al. Ligamentous Injuries and the Risk of Associated Tissue Damage in Acute Ankle Sprains in Athletes: A Cross-sectional MRI Study. Am J Sports Med 2014;42(7):1549–57.
29. Joshy S, Abdulkadir U, Chaganti S, et al. Accuracy of MRI scan in the diagnosis of ligamentous and chondral pathology in the ankle. Foot Ankle Surg 2010;16(2):78–80.

30. Oae K, Takao M, Uchio Y, et al. Evaluation of anterior talofibular ligament injury with stress radiography, ultrasonography and MR imaging. Skeletal Radiol 2010;39(1):41–7.
31. Yi J, Lee YH, Hahn S, et al. Fast isotropic volumetric magnetic resonance imaging of the ankle: Acceleration of the three-dimensional fast spin echo sequence using compressed sensing combined with parallel imaging. Eur J Radiol 2019; 112:52–8.
32. Yi J, Cha JG, Lee YK, et al. MRI of the anterior talofibular ligament, talar cartilage and os subfibulare: Comparison of isotropic resolution 3D and conventional 2D T2-weighted fast spin-echo sequences at 3.0 T. Skeletal Radiol 2016;45(7): 899–908.
33. Park HJ, Lee SY, Choi YJ, et al. 3D isotropic T2-weighted fast spin echo (VISTA) versus 2D T2-weighted fast spin echo in evaluation of the calcaneofibular ligament in the oblique coronal plane. Clin Radiol 2017;72(2):176 e1–e7.
34. Choo HJ, Lee SJ, Kim DW, et al. Multibanded anterior talofibular ligaments in normal ankles and sprained ankles using 3D isotropic proton density-weighted fast spin-echo MRI sequence. AJR Am J Roentgenol 2014;202(1):W87–94.
35. Akatsuka Y, Teramoto A, Takashima H, et al. Morphological evaluation of the calcaneofibular ligament in different ankle positions using a three-dimensional MRI sequence. Surg Radiol Anat 2019;41(3):307–11.
36. Clanton TO, Porter DA. Primary care of foot and ankle injuries in the athlete. Clin Sports Med 1997;16(3):435–66.
37. Kofotolis ND, Kellis E, Vlachopoulos SP. Ankle sprain injuries and risk factors in amateur soccer players during a 2-year period. Am J Sports Med 2007;35(3): 458–66.
38. Chun KY, Choi YS, Lee SH, et al. Deltoid Ligament and Tibiofibular Syndesmosis Injury in Chronic Lateral Ankle Instability: Magnetic Resonance Imaging Evaluation at 3T and Comparison with Arthroscopy. Korean J Radiol 2015;16(5): 1096–103.
39. Crim JR, Beals TC, Nickisch F, et al. Deltoid ligament abnormalities in chronic lateral ankle instability. Foot Ankle Int 2011;32(9):873–8.
40. Mengiardi B, Zanetti M, Schottle PB, et al. Spring ligament complex: MR imaging-anatomic correlation and findings in asymptomatic subjects. Radiology 2005; 237(1):242–9.
41. Nussbaum ED, Hosea TM, Sieler SD, et al. Prospective evaluation of syndesmotic ankle sprains without diastasis. Am J Sports Med 2001;29(1):31–5.
42. Bencardino J, Rosenberg ZS, Delfaut E. MR imaging in sports injuries of the foot and ankle. Magn Reson Imaging Clin N Am 1999;7(1):131–49, ix.
43. Espinosa N, Smerek JP, Myerson MS. Acute and chronic syndesmosis injuries: pathomechanisms, diagnosis and management. Foot Ankle Clin 2006;11(3): 639–57.
44. Sman AD, Hiller CE, Refshauge KM. Diagnostic accuracy of clinical tests for diagnosis of ankle syndesmosis injury: a systematic review. Br J Sports Med 2013;47(10):620–8.
45. Rammelt S, Zwipp H, Grass R. Injuries to the distal tibiofibular syndesmosis: an evidence-based approach to acute and chronic lesions. Foot Ankle Clin 2008; 13(4):611–33, vii-viii.
46. Ogilvie-Harris DJ, Gilbart MK, Chorney K. Chronic pain following ankle sprains in athletes: the role of arthroscopic surgery. Arthroscopy 1997;13(5):564–74.
47. Czajka CM, Tran E, Cai AN, et al. Ankle sprains and instability. Med Clin North Am 2014;98(2):313–29.

48. Oae K, Takao M, Naito K, et al. Injury of the tibiofibular syndesmosis: value of MR imaging for diagnosis. Radiology 2003;227(1):155–61.
49. Hermans JJ, Ginai AZ, Wentink N, et al. The additional value of an oblique image plane for MRI of the anterior and posterior distal tibiofibular syndesmosis. Skeletal Radiol 2011;40(1):75–83.
50. Kim M, Choi YS, Jeong MS, et al. Comprehensive Assessment of Ankle Syndesmosis Injury Using 3D Isotropic Turbo Spin-Echo Sequences: Diagnostic Performance Compared With That of Conventional and Oblique 3-T MRI. AJR Am J Roentgenol 2017;208(4):827–33.
51. Myerson MS, Thordarson DB, Johnson JE, et al. Classification and Nomenclature: Progressive Collapsing Foot Deformity. Foot Ankle Int 2020;41(10):1271–6.
52. Chhabra A, Soldatos T, Chalian M, et al. 3-Tesla magnetic resonance imaging evaluation of posterior tibial tendon dysfunction with relevance to clinical staging. J Foot Ankle Surg 2011;50(3):320–8.
53. O'Neil JT, Pedowitz DI, Kerbel YE, et al. Peroneal Tendon Abnormalities on Routine Magnetic Resonance Imaging of the Foot and Ankle. Foot Ankle Int 2016;37(7):743–7.
54. Saxena A, Luhadiya A, Ewen B, et al. Magnetic resonance imaging and incidental findings of lateral ankle pathologic features with asymptomatic ankles. J Foot Ankle Surg 2011;50(4):413–5.
55. Fallat L, Grimm DJ, Saracco JA. Sprained ankle syndrome: prevalence and analysis of 639 acute injuries. J Foot Ankle Surg 1998;37(4):280–5.
56. Berndt AL, Harty M. Transchondral fractures (osteochondritis dissecans) of the talus. J Bone Joint Surg Am 1959;41-A:988–1020.
57. Rikken QGH, Kerkhoffs G. Osteochondral Lesions of the Talus: An Individualized Treatment Paradigm from the Amsterdam Perspective. Foot Ankle Clin 2021;26(1):121–36.
58. Hannon CP, Smyth NA, Murawski CD, et al. Osteochondral lesions of the talus: aspects of current management. Bone Joint Lett J 2014;96-B(2):164–71.
59. Mintz DN, Tashjian GS, Connell DA, et al. Osteochondral lesions of the talus: a new magnetic resonance grading system with arthroscopic correlation. Arthroscopy 2003;19(4):353–9.
60. Verhagen RA, Maas M, Dijkgraaf MG, et al. Prospective study on diagnostic strategies in osteochondral lesions of the talus. Is MRI superior to helical CT? J Bone Joint Surg Br 2005;87(1):41–6.
61. Shakoor D, Guermazi A, Kijowski R, et al. Diagnostic Performance of Three-dimensional MRI for Depicting Cartilage Defects in the Knee: A Meta-Analysis. Radiology 2018;289(1):71–82.
62. Ulbrich EJ, Zubler V, Sutter R, et al. Ligaments of the Lisfranc joint in MRI: 3D-SPACE (sampling perfection with application optimized contrasts using different flip-angle evolution) sequence compared to three orthogonal proton-density fat-saturated (PD fs) sequences. Skeletal Radiol 2013;42(3):399–409.
63. Kim TH, Moon SG, Jung HG, et al. Subtalar instability: imaging features of subtalar ligaments on 3D isotropic ankle MRI. BMC Musculoskelet Disord 2017;18(1):475.
64. Choo HJ, Suh JS, Kim SJ, et al. Ankle MRI for anterolateral soft tissue impingement: increased accuracy with the use of contrast-enhanced fat-suppressed 3D-FSPGR MRI. Korean J Radiol 2008;9(5):409–15.
65. Zhang Y, He X, Li J, et al. An MRI study of the tibial nerve in the ankle canal and its branches: a method of multiplanar reformation with 3D-FIESTA-C sequences. BMC Med Imaging 2021;21(1):51. https://doi.org/10.1186/s12880-021-00582-8.